Meissner-like Effect for a Synthetic Gauge Field in Multimode Cavity QED

Kyle E. Ballantine,[1] Benjamin L. Lev,[2] and Jonathan Keeling[1]
[1]SUPA, School of Physics and Astronomy, University of St. Andrews, St. Andrews KY16 9SS, United Kingdom
[2]Departments of Physics and Applied Physics and Ginzton Laboratory, Stanford University, Stanford, California 94305, USA
(Received 25 August 2016; published 27 January 2017)

Previous realizations of synthetic gauge fields for ultracold atoms do not allow the spatial profile of the field to evolve freely. We propose a scheme which overcomes this restriction by using the light in a multimode cavity with many nearly degenerate transverse modes, in conjunction with Raman coupling, to realize an artificial magnetic field which acts on a Bose-Einstein condensate of neutral atoms. We describe the evolution of such a system and present the results of numerical simulations which show dynamical coupling between the effective field and the matter on which it acts. Crucially, the freedom of the spatial profile of the field is sufficient to realize a close analogue of the Meissner effect, where the magnetic field is expelled from the superfluid. This backaction of the atoms on the synthetic field distinguishes the Meissner-like effect described here from the Hess-Fairbank suppression of rotation in a neutral superfluid observed elsewhere.

DOI: 10.1103/PhysRevLett.118.045302

The Meissner effect [1] is the *sine qua non* of superconductivity [2]. As captured by the Ginzburg-Landau equations [3], the superfluid order parameter couples to the electromagnetic fields such that there is perfect diamagnetism. Physically, this arises because the normal paramagnetic response of matter is completely suppressed by the phase stiffness of the superfluid, leaving only the diamagnetic current [4]. The magnetic field thus decays exponentially into the bulk [5]. Exponentially decaying fields are symptomatic of a massive field theory and so can be seen as a direct consequence of the Anderson-Higgs mechanism [6,7] giving the electromagnetic field a mass gap. Central to all these phenomena is that minimal coupling between the electromagnetic field and the superfluid modifies the equations of motion for both the superfluid and the electromagnetic field.

The concept of "synthetic" gauge fields has attracted much attention over the past few years. In the context of ultracold atoms, realizations have included schemes based on dark states [8,9] or Raman driving [10–12] or inducing Peierls phases in lattice systems [13–23] (for a review, see [24–27]). There have also been proposals to realize gauge fields for photons, including "free space" realizations using Rydberg atoms in nonplanar ring cavity geometries [28] as well as Peierls phases for photon hopping in coupled cavity arrays [29–31]. However, with a few exceptions, all these have involved static gauge fields—there is no feedback of the atoms (or photons) on the synthetic field. Thus, even in the pioneering demonstration of a Meissner phase of chiral currents [23], it is noted that these experiments are closer to the Hess-Fairbank effect [32] (suppression of rotation in a neutral superfluid) and do not show an expulsion of the synthetic field. In contrast, a charged superfluid acts back on the magnetic field.

The synthetic field cannot be expelled in the above schemes, because it is set by a fixed external laser or the system geometry. The exceptions are thus proposals where the strength of the synthetic field depends on a dynamical quantity. One such proposal is in optomechanical cavity arrays with a Peierls phase for photon hopping set by mechanical oscillators [33]. Another proposal is to consider atoms in optical cavities, replacing the external laser drive by light in the cavity, as has been recently proposed by Zheng and Cooper [34], with a two-photon-assisted hopping scheme involving the cavity and a transverse pump. This scheme naturally relates to the self-organization of atoms under transverse pumping [35–37] and proposed extensions involving spin-orbit coupling [38–42] and self-organized chiral states [43,44]. However, in these schemes, a single-mode cavity is used, giving a "mean-field" coupling due to the infinite-range nature of the interactions, and not the local coupling to the gauge potential present in the Ginzburg-Landau equations.

Locality can be restored in a multimode cavity—in a cavity that supports multiple nearly degenerate transverse modes, one can build localized wave packets [45]. This is also illustrated for a longitudinally pumped system when considering the Talbot effect [46] with cold atoms [47]: When atoms are placed in front of a planar mirror and illuminated with coherent light, the phase modulation of the light is transformed by propagation into intensity modulation, leading to self-organization. This effect can be viewed as an effective atom-atom interaction mediated by light, leading to density-wave formation [48–50]. In this Letter, we show how multimode cavity QED [45,51–54] can be used to realize a dynamical gauge field for cold atoms capable of realizing an analogue of the Meissner effect for charged superfluids. The simultaneous presence of near-degenerate cavity modes allows the spatial intensity profile of the cavity light field to change over time in response to the state of the atoms, in a form directly analogous to the Ginzburg-Landau equations.

By realizing such a multimode cavity QED simulator of matter and dynamical gauge fields, numerous possibilities arise. Most intriguingly, the tunability of the parameters controlling the effective matter-light coupling potentially allow one to simulate the behavior of matter with alternate values of the fine structure constant α. This could provide a continuum gauge field theory simulator complementary to the proposals for simulating lattice gauge field theories using ultracold atoms [55–65], trapped ions [66–69], or superconducting circuits [70,71]. Other opportunities arising from our work are to explore the differences between Bose-condensed, thermal, and fermionic atoms in the geometry considered above: The Meissner effect depends on the phase stiffness of superfluid atoms and so should vanish at higher temperatures. For fermions, one might use synthetic field expulsion as a probe of BCS superfluidity.

Our proposal is based on the confocal cavity system recently realized by Kollár *et al.* [53,54]. This cavity may be tuned between confocal multimode and single-mode configurations. In addition, light can be pumped transversely or longitudinally and patterned using a digital light modulator [72]. Multimode cavity QED has previously been proposed to explore beyond mean-field physics in the self-organization of ultracold atoms [45,51,54].

We consider this cavity in the near-confocal case, so that many modes are near degenerate. This cavity contains a 2D condensate of atoms confined along the cavity axis as shown in Fig. 1. These atoms have two low-lying internal states, $|A\rangle$ and $|B\rangle$, which are coupled by two counter-propagating Raman beams via a higher intermediate state; for example, considering bosonic ^{87}Rb, one may create an effective two-level system from three $F=1$ levels by noting that the $m=\pm 1$ levels, split by a magnetic field [10,12], can be coupled via the $m=0$ state, which can be off resonant due to the quadratic Zeeman shift ϵ, as previously shown in Refs. [12,73]. If the population of the excited state is negligible, the Raman beams lead to an effective Rabi coupling $\Omega \propto (\prod_{i=1}^{4}\Omega_i)/\Delta_A^2\epsilon$ between the two lower states, which in the scheme suggested in Fig. 1 is fourth order and where Δ_A is the effective detuning from the excited states. An atom in state $|A\rangle$ gains momentum $q\hat{x}$ by absorbing two photons from one transverse beam and loses momentum $-q\hat{x}$ by emitting two photons into the other beam, finishing in state $|B\rangle$, where $q/2 = 2\pi/\lambda$ is the momentum of the Raman beams. Hence, the two states have momentum differing by $2q\hat{x}$. Crucially, each state has a different Stark shift due to the interaction with many cavity photons contributing to the intensity I, with coefficients $\mathcal{E}_{A,B}$. This gives an atomic Hamiltonian of the form $\hat{H}_{\text{atom}} = \int d^2\mathbf{r}dz\tilde{\Psi}^{\dagger}_{\mathbf{r},z}[\mathbf{h} + V_{\text{ext}}(\mathbf{r},z)]\tilde{\Psi}_{\mathbf{r},z} + \hat{H}_{\text{int}}$, where

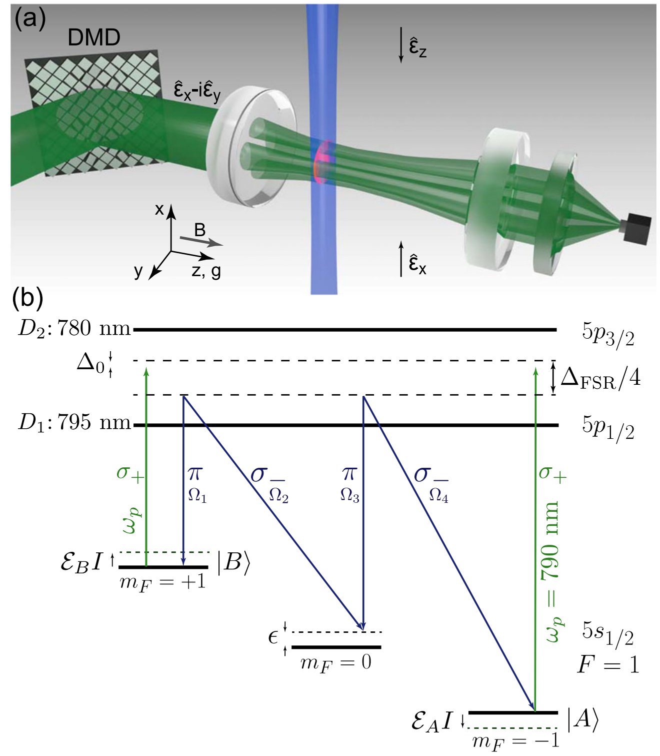

FIG. 1. (a) A 2D Bose-Einstein condensate (BEC) is coupled to linearly polarized counterpropagating Raman beams in $\hat{x}$ and trapped inside a cavity set in the multimode, confocal configuration. (Optical trapping lasers are not shown, and only TEM_{10} and TEM_{01} modes are shown for simplicity.) The axis of the oblate BEC is collinear with the cavity axis. The cavity, with field loss κ, is pumped along $+\hat{z}$ by a circularly polarized field of frequency ω_p detuned by Δ_0 from the confocal cavity frequency ω_0. The pump laser is spatially shaped with a digital multimirror device (DMD) spatial light modulator before cavity injection. Cavity light is imaged by an EMCCD camera. (The atomic absorption imaging laser and camera are not shown.) A magnetic field B is oriented along $+\hat{z}$. (b) ^{87}Rb atomic level diagram with three coupling lasers shown. Green arrows show the pump field that Stark shifts the state $|A\rangle$ and $|B\rangle$ by $\mathcal{E}_{A,B}$. The laser frequency is set to the tune-out wavelength between the D_1 and D_2 lines in ^{87}Rb. The blue arrows show the two-photon Raman-coupling fields driving π and σ_- transitions—effected by obeying electric dipole selection rules for the polarizations given in (a)—with Rabi frequencies Ω_i. The Raman fields are detuned from ω_0 by a quarter of a free spectral range $\Delta_{\text{FSR}}/4$ and the $m=0$ state is detuned by ϵ via the quadratic Zeeman shift.

$$\mathbf{h} = \begin{pmatrix} \frac{(-i\nabla - q\hat{\mathbf{x}})^2}{2m} - \mathcal{E}_A I(\mathbf{r},z) & \Omega/2 \\ \Omega/2 & \frac{(-i\nabla + q\hat{\mathbf{x}})^2}{2m} - \mathcal{E}_B I(\mathbf{r},z) \end{pmatrix}. \quad (1)$$

For simplicity, here and in the following, we write $\mathbf{r} = (x, y)$, with the z dependence written separately, and set $\hbar = 1$. The term $\hat{H}_{\text{int}}$ describes contact interactions between atoms with strength U.

The cavity pump field wavelength is set to be at the "tune-out" point, 790.018 nm, between the D_1 and D_2 lines in ^{87}Rb [74]. The scalar light shift is zero at this wavelength, which means that the atom-trapping frequencies are nearly unaffected by the cavity light in the absence of Raman coupling. The vector light shift is approximately equal and opposite for states $|A\rangle$ and $|B\rangle$ due to their opposite m_F projections, i.e., $\mathcal{E}_A = -\mathcal{E}_B$. Spontaneous emission is low, less than $\sim$10 Hz for the required Stark shifts, since this light is far detuned from either excited state. The Raman coupling scheme is identical to those in Refs. [12,73] that exhibited nearly 0.5-s spontaneous-emission-limited BEC lifetimes. The Raman lasers do not scatter into the cavity, since they are detuned $\Delta_{\mathrm{FSR}}/4 = 3.25$ GHz from any family of degenerate cavity modes for an $L = 1$-cm confocal cavity [53]. The BEC lifetime under our cavity and Raman-field dressing scheme should therefore be more than 100 ms, sufficient to observe the predicted physics.

The artificial magnetic field that arises from the Raman driving scheme is in $\hat{z}$ [10], and so the interesting atomic dynamics will be in the transverse ($\hat{x}$-$\hat{y}$) plane. We therefore consider a 2D pancake of atoms, with strong trapping in $\hat{z}$, such that we may write $\Psi_{A,B}(\mathbf{r},z) = \psi_{A,B}(\mathbf{r})Z(z)$, where $Z(z)$ is a narrow Gaussian profile due to the strong trapping in $\hat{z}$. In this strong trapping limit, we can integrate out the z dependence to produce effective equations of motion for the transverse wave functions $\psi_{A,B}$ and the transverse part of the cavity light field φ. We consider the case where the atom cloud is trapped near one end of the cavity, $z_0 \simeq \pm z_R$, as this leads to a quasilocal coupling between atoms and cavity light (see Supplemental Material [75] for details). We choose to normalize the atomic wave functions such that $\int d^2\mathbf{r}(|\psi_A|^2 + |\psi_B|^2) = 1$, so that the number of atoms N appears explicitly. The transverse equations of motion then take the form

$$i\partial_t\varphi = \left[\frac{\delta}{2}\left(-l^2\nabla^2 + \frac{r^2}{l^2}\right) - \Delta_0 - i\kappa - N\mathcal{E}_\Sigma(|\psi_A|^2 + |\psi_B|^2) - N\mathcal{E}_\Delta(|\psi_A|^2 - |\psi_B|^2)\right]\varphi + f(\mathbf{r}), \quad (2)$$

$$i\partial_t\begin{pmatrix}\psi_A\\ \psi_B\end{pmatrix} = \left[-\frac{\nabla^2}{2m} + V_{\mathrm{ext}}(\mathbf{r}) - \mathcal{E}_\Sigma|\varphi|^2 + NU(|\psi_A|^2 + |\psi_B|^2) + \begin{pmatrix}-\mathcal{E}_\Delta|\varphi|^2 + i\frac{q}{m}\partial_x & \Omega/2\\ \Omega/2 & \mathcal{E}_\Delta|\varphi|^2 - i\frac{q}{m}\partial_x\end{pmatrix}\right]\begin{pmatrix}\psi_A\\ \psi_B\end{pmatrix}. \quad (3)$$

Here we have rewritten $\mathcal{E}_\Sigma = (\mathcal{E}_A + \mathcal{E}_B)/4$ and $\mathcal{E}_\Delta = (\mathcal{E}_A - \mathcal{E}_B)/4$. $\Delta_0 = \omega_P - \omega_0$ is the detuning of the pump from the confocal cavity frequency ω_0, and $f(\mathbf{r})$ is the pump profile. We are considering modes in a nearly confocal cavity for the cavity field φ [53]. In such a case, a given family of nearly degenerate modes takes the form of either even or odd Gauss-Hermite functions, where $\sqrt{2}l$ is the beam waist [76]. The first term in Eq. (2) is the real-space operator describing the splitting between the nearly degenerate modes when the cavity is detuned away from confocality with mode splitting δ. The restriction to only even modes means we must restrict to $\varphi(\mathbf{r}) = \varphi(-\mathbf{r})$; however, Eqs. (2) and (3) preserve this symmetry if it is initially present.

We first describe in general terms the behavior we can expect from Eqs. (2) and (3) before discussing the full steady state of these equations. As this model is closely related to that proposed by Spielman [10], one may expect the same behavior to occur [12]. Namely, if we construct a basis transformation between the original levels and the dressed states $(\psi_+, \psi_-)^T = S(\psi_A, \psi_B)^T$ such that the atomic Hamiltonian is diagonalized, then atoms in each of these dressed states see effective (opposite) magnetic fields. The dispersion relation for the lower manifold (i.e., the noninteracting and translationally invariant part of the energy) has the form

$$E_-(\mathbf{k}) = \frac{1}{2m^*}(\mathbf{k} - Q|\varphi|^2\hat{\mathbf{x}})^2 - \mathcal{E}_\Sigma|\varphi|^2 - \mathcal{E}_4|\varphi|^4 + \cdots, \quad (4)$$

which depends on the cavity light intensity $|\varphi|^2$. This can be recognized as the energy of a particle in a magnetic vector potential $\mathbf{A} = |\varphi|^2\hat{\mathbf{x}}$ with effective charge $Q = 2\mathcal{E}_\Delta q/(\Omega - 2q^2/m)$. The effective field experienced by the atoms is therefore proportional to the difference in the Stark shifts experienced by each level, as the average Stark shift simply leads to a scalar potential $\mathcal{E}_\Sigma|\varphi|^2$. The atoms acquire an effective mass $m^* = m\Omega/(\Omega - 2q^2/m)$, because the eigenstate is in a superposition of states with differing momenta $k \pm q\hat{x}$. Finally, there is an additional scalar potential term proportional to $\mathcal{E}_4 = \mathcal{E}_\Delta^2/(\Omega - 2q^2/m)$, because each component experiences a different Stark shift. As $\Omega \to \infty$, the eigenstate approaches a symmetric superposition, the effective mass approaches m, and the extra scalar potential disappears.

As compared to Refs. [10,12], the crucial difference in Eqs. (2) and (3) is that the atomic dynamics also acts back on the cavity light field φ. We can explore the nature of this backaction by expanding the low-energy eigenstate ψ_- to first order in $1/\Omega$. In the low-energy manifold, the difference $|\psi_A|^2 - |\psi_B|^2$ in Eq. (2) can be related to the wave function ψ_- by

$$|\psi_A|^2 - |\psi_B|^2 = \frac{q}{im\Omega}(\psi_-^*\partial_x\psi_- - \psi_-\partial_x\psi_-^*) + \frac{2\mathcal{E}_\Delta}{\Omega}|\psi_-|^2|\varphi|^2. \quad (5)$$

This has exactly the expected form of the effect of charged particles on a vector potential: There is a current-dependent

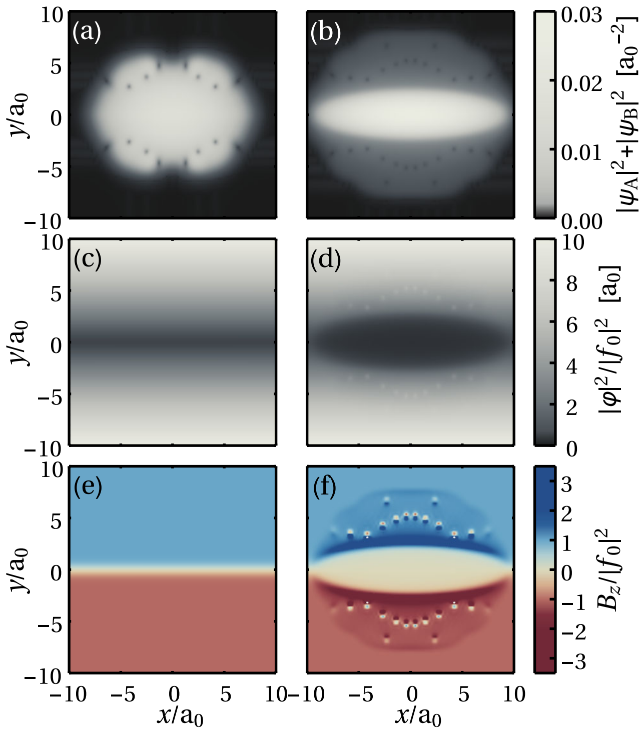

FIG. 2. (a) Ground state of the condensate in a static field $|\varphi|^2 \propto |y|$ showing vortex formation. (b) Density of the condensate when the field is allowed to evolve. No vortices remain in the cloud. (c) Relative intensity (i.e., $|\varphi|^2/|f_0|^2$) of light in a cavity with no atom-light coupling used to generate (a). (d) Steady-state relative intensity of light when coupled to an atomic cloud, showing a reduction in the region where atoms are present. Vortices remain in the region of low atomic density where the intensity recovers and so the magnetic field is high. (e) Applied magnetic field [derivative of the intensity in (c)] and (f) magnetic field after coupled evolution showing the applied field has been expelled from the condensate. All lengths are in units of the harmonic oscillator length $a_0 = 1/\sqrt{m\omega_x}$. Using ω_x as the frequency unit, other parameters are given by $\delta = -10$, $l = 1$, $\Delta_0 = -50$, $\kappa = 1000$, $\mathcal{E}_\Delta = 50$, $q = 70$, $\Omega = 10^5$, $mU = 1.5 \times 10^{-3}$, $N = 10^6$, and $f_0 = 4$, all relevant for the cavity considered in Refs. [53,54].

term, the first term, followed by a diamagnetic term. The current-dependent term appearing in Eq. (2) would lead to a paramagnetic response. However, in a superfluid state, this contribution is suppressed due to the phase stiffness of the superfluid, and the surviving diamagnetic term then leads to the Meissner effect.

This diamagnetic response is shown in Fig. 2. Here we consider a source term $f(\mathbf{r})$, the pump field, which, in the absence of atoms, we set to have an intensity profile such that $|\varphi|^2 \propto |y|$, and thus the magnetic field has uniform magnitude, but with a sign dependent on y (see Supplemental Material [75]). The applied effective magnetic field is $B_z = \partial_y|\varphi|^2 \approx \pm|f_0|^2$, where f_0 is a constant which specifies the overall amplitude of the pump. The rows of Fig. 2 show the atomic density, the cavity intensity, and the artificial magnetic field, respectively. The left column shows the case where the field is artificially kept static, i.e., where the terms proportional to $\psi_{A,B}$ are omitted from Eq. (2) to prevent any feedback, and the right column shows the case when the field is allowed to evolve.

As expected, in Fig. 2(f), we see that with the feedback included the magnetic field is suppressed in the region containing the atomic cloud. Compared to the applied field [Fig. 2(e)], the field is suppressed in a large area where the atomic density, shown in Fig. 2(b), is high. This is a consequence of the change in the cavity field which goes from being linear in $|y|$, as shown in Fig. 2(c), to having a region of near constant value, shown in Fig. 2(d). This change in the intensity profile can be measured directly, and so the expulsion of the effective field can be reconstructed from the light emitted from the cavity. Additionally, as the cavity light intensity recovers to its default value, this causes an increase in its gradient, and so in Fig. 2(f) one sees that the artificial magnetic field is increased immediately outside the atom cloud. In response to the changing field, we see that while in Fig. 2(a) there are vortices due to the static field, in Fig. 2(b) the higher density region no longer contains vortices, although they remain around the edges of the condensate where there is still a high magnetic field. As in the case of the standard Abrikosov vortex lattice, the density of vortices depends on the local field strength, and the spacing goes from being larger than the size of the cloud to much smaller as the field recovers to its default value. This reduction in field $|\varphi|$ also leads to a change in the geometric scalar potential terms in Eq. (4), which is what causes the condensate to shrink in size (see also below). Further out, the condensate density decays slowly in $\hat{y}$, and the remaining vortices lead to small modulations in the intensity. However, these modulations over small areas lead to quite large derivatives which show up as flux-antiflux pairs.

While the results in Fig. 2 clearly show a suppression of the magnetic field analogous to the Meissner effect, it is important to note several differences between Eqs. (2) and (3) and the standard Meissner effect. In particular, while the atoms see an effective vector potential $|\varphi|^2\hat{\mathbf{x}}$, the remaining action for the field $|\varphi|^2$ does not simulate the Maxwell action for a gauge field: The remaining action does not have gauge symmetry and has a small residual gap (due to the cavity loss and detuning). Because the action for φ is not gapless, there is already an exponential decay of the synthetic field away from its source. What our results show is that coupling to a superfluid significantly enhances the gap for this field (in our case, by at least one order of magnitude), thus leading to a significant suppression of the field in the region where the atoms live. These differences mean that the distinction between type I and type II superconductivity is not clear. These points are discussed further in Ref. [75]. The effect of increasing the effective magnetic field strength is shown in the figure.

The figures are the result of numerical simulations of Eqs. (2) and (3) performed by using XMDS2 (extensible multidimensional simulator) [77]. They represent the steady state which is reached when the artificial magnetic field, proportional to the pump amplitude, is adiabatically increased from zero. A computationally efficient way to find this is to evolve the equation of motion for the light field, which includes pumping and loss, in real time while simultaneously evolving the equation of motion for the condensate in imaginary time and renormalizing this wave function at each step. Hence, we find a state which is both a steady state of the real-time equations of motion and also the ground state for the atoms in that given intensity profile. This method correctly finds the steady-state profile, but the transient dynamics does not match that which would be seen experimentally, as we focus here only on the steady states. See Supplemental video and Ref. [75] for the real-time evolution. We make use of the natural units of length and frequency set by the harmonic trap, i.e., $a_0 = 1/\sqrt{m\omega_x}$ and ω_x. For realistic experimental parameters, ω_x may be on the order of 1 kHz and $a_0 \approx 1\ \mu$m. The values of all other parameters are given in the figure captions.

The change in shape of the condensate in Fig. 2(b) can be explained by our choice of potential $V_{\rm ext}(\mathbf{r})$. As is clear from Eq. (4), the field φ leads to both vector and scalar potential terms. The scalar potentials have two contributions: quadratic and quartic. Analogous to the centrifugal force on a rotating condensate, these terms lead to a reduction (or even reversal) of the transverse harmonic trapping of the atoms. As a consequence of working at the tune-out wavelength, the quadratic scalar potentials in Eq. (4) are zero, i.e., $\mathcal{E}_\Sigma = 0$. The quartic term is harder to eliminate, but its effects can be compensated by choosing a trap of the form

$$V_{\rm ext} = \frac{m\omega_x^2}{2}(x^2 + y^2) + \mathcal{E}_4|f_0|^4 y^2, \tag{6}$$

i.e., an asymmetric harmonic oscillator potential with $\omega_y = \sqrt{\omega_x^2 + 2\mathcal{E}_4|f_0|^2/m}$. However, this expression assumes $|\varphi|^2 = |f_0|^2|y|$, as would hold in the absence of atomic diamagnetism. As the magnetic field is expelled, the scalar potential also changes, and the condensate becomes more tightly trapped.

Figure 3 shows cross sections at $x = 0$ of (a) the atomic density and (b) the artificial magnetic field for various values of the total number of atoms. Increasing the number of atoms leads to a larger condensate with a lower peak density (the integral of density remains normalized). The resulting magnetic field profile is shown in Fig. 3(b). The area of low magnetic field is closely aligned to the area of high atomic density. At the edges of the cloud, the artificial field is increased as the expelled field accumulates here before returning to its default value well outside the cloud. The effect of vortices in the very low density areas can also

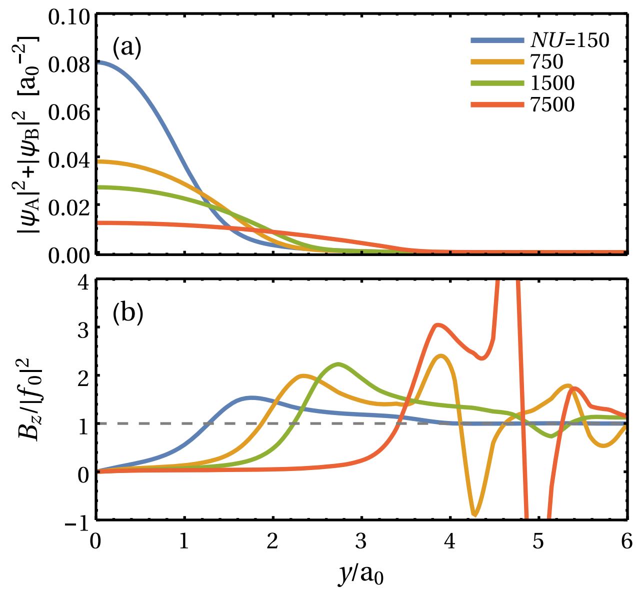

FIG. 3. Profile of the (a) atomic density and (b) artificial field with varying numbers of atoms, in terms of the dimensionless parameter mNU. For realistic values, this corresponds to $N = 10^5$ (blue curve), $N = 5\times 10^5$ (yellow curve), $N = 10^6$ (green curve), and $N = 5\times 10^6$ (orange curve). All other parameters are the same as in Fig. 2.

be seen. Varying other parameters leads to similar physics, which can be understood in terms of the effective parameters introduced in Eq. (4). The effect of varying the effective field strength is discussed further in Ref. [75].

In summary, we have shown how a spatially varying synthetic gauge field can be achieved and how magnetic field suppression in an atomic superfluid, analogous to the Meissner effect, can be realized. By effecting an artificial magnetic field proportional to the intensity of light in a multimode cavity, we have coupled the dynamics of the spatial profile of the magnetic field and the atomic wave function. Our results illustrate the potential of multimode cavity QED to simulate dynamical gauge fields and to explore self-consistent steady states, and potentially phase transitions, of matter coupled to synthetic gauge fields.

We acknowledge helpful discussions with E. Altman, M. J. Bhaseen, S. Gopalakrishnan, B. D. Simons, and I. Spielman. We thank V. D. Vaidya and Y. Guo for help in preparation of the manuscript. K. E. B. and J. K. acknowledge support from EPSRC program TOPNES (EP/I031014/1). J. K. acknowledges support from the Leverhulme Trust (IAF-2014-025). B. L. L. acknowledges support from the ARO and the David and Lucile Packard Foundation.

[1] W. Meissner and R. Ochsenfeld, Naturwissenschaften **21**, 787 (1933).
[2] A. Leggett, *Quantum Liquids: Bose Condensation and Cooper Pairing in Condensed-Matter Systems*, Oxford

Graduate Texts in Mathematics (Oxford University, New York, 2006).
[3] V. L. Ginzburg and L. D. Landau, Zh. Eksp. Teor. Fiz. **20**, 1064 (1950).
[4] J. R. Schrieffer, *Theory of Superconductivity* (Westview Press, Boulder, CO, 1983).
[5] F. London and H. London, Proc. R. Soc. A **149**, 71 (1935).
[6] P. W. Anderson, Phys. Rev. **130**, 439 (1963).
[7] P. W. Higgs, Phys. Rev. Lett. **13**, 508 (1964).
[8] P. M. Visser and G. Nienhuis, Phys. Rev. A **57**, 4581 (1998).
[9] G. Juzeliūnas and P. Öhberg, Phys. Rev. Lett. **93**, 033602 (2004).
[10] I. B. Spielman, Phys. Rev. A **79**, 063613 (2009).
[11] Y.-J. Lin, R. L. Compton, A. R. Perry, W. D. Phillips, J. V. Porto, and I. B. Spielman, Phys. Rev. Lett. **102**, 130401 (2009).
[12] Y.-J. Lin, R. L. Compton, K. Jimenez-Garcia, J. V. Porto, and I. B. Spielman, Nature (London) **462**, 628 (2009).
[13] D. Jaksch and P. Zoller, New J. Phys. **5**, 56 (2003).
[14] A. S. Sørensen, E. Demler, and M. D. Lukin, Phys. Rev. Lett. **94**, 086803 (2005).
[15] A. R. Kolovsky, Europhys. Lett. **93**, 20003 (2011).
[16] N. R. Cooper, Phys. Rev. Lett. **106**, 175301 (2011).
[17] J. Struck, C. Ölschläger, R. Le Targat, P. Soltan-Panahi, A. Eckardt, M. Lewenstein, P. Windpassinger, and K. Sengstock, Science **333**, 996 (2011).
[18] M. Aidelsburger, M. Atala, S. Nascimbène, S. Trotzky, Y.-A. Chen, and I. Bloch, Phys. Rev. Lett. **107**, 255301 (2011).
[19] P. Hauke, O. Tieleman, A. Celi, C. Ölschläger, J. Simonet, J. Struck, M. Weinberg, P. Windpassinger, K. Sengstock, M. Lewenstein, and A. Eckardt, Phys. Rev. Lett. **109**, 145301 (2012).
[20] J. Struck, C. Ölschläger, M. Weinberg, P. Hauke, J. Simonet, A. Eckardt, M. Lewenstein, K. Sengstock, and P. Windpassinger, Phys. Rev. Lett. **108**, 225304 (2012).
[21] H. Miyake, G. A. Siviloglou, C. J. Kennedy, W. C. Burton, and W. Ketterle, Phys. Rev. Lett. **111**, 185302 (2013).
[22] M. Aidelsburger, M. Atala, M. Lohse, J. T. Barreiro, B. Paredes, and I. Bloch, Phys. Rev. Lett. **111**, 185301 (2013).
[23] M. Atala, M. Aidelsburger, M. Lohse, J. T. Barreiro, B. Paredes, and I. Bloch, Nat. Phys. **10**, 588 (2014).
[24] J. Dalibard, F. Gerbier, G. Juzeliūnas, and P. Öhberg, Rev. Mod. Phys. **83**, 1523 (2011).
[25] N. Goldman, G. Juzeliūnas, P. Öhberg, and I. B. Spielman, Rep. Prog. Phys. **77**, 126401 (2014).
[26] H. Zhai, Int. J. Mod. Phys. B **26**, 1230001 (2012).
[27] H. Zhai, Rep. Prog. Phys. **78**, 026001 (2015).
[28] N. Schine, A. Ryou, A. Gromov, A. Sommer, and J. Simon, Nature (London) **534**, 671 (2016).
[29] K. Fang, Z. Yu, and S. Fan, Nat. Photonics **6**, 782 (2012).
[30] M. Hafezi, S. Mittal, J. Fan, A. Migdall, and J. M. Taylor, Nat. Photonics **7**, 1001 (2013).
[31] T. Dubček, K. Lelas, D. Jukić, R. Pezer, M. Soljačić, and H. Buljan, New J. Phys. **17**, 125002 (2015).
[32] G. B. Hess and W. M. Fairbank, Phys. Rev. Lett. **19**, 216 (1967).
[33] S. Walter and F. Marquardt, New J. Phys. **18**, 113029 (2016).
[34] W. Zheng and N. R. Cooper, Phys. Rev. Lett. **117**, 175302 (2016).
[35] P. Domokos and H. Ritsch, Phys. Rev. Lett. **89**, 253003 (2002).
[36] A. T. Black, H. W. Chan, and V. Vuletić, Phys. Rev. Lett. **91**, 203001 (2003).
[37] K. Baumann, C. Guerlin, F. Brennecke, and T. Esslinger, Nature (London) **464**, 1301 (2010).
[38] Y. Deng, J. Cheng, H. Jing, and S. Yi, Phys. Rev. Lett. **112**, 143007 (2014).
[39] L. Dong, L. Zhou, B. Wu, B. Ramachandhran, and H. Pu, Phys. Rev. A **89**, 011602 (2014).
[40] B. Padhi and S. Ghosh, Phys. Rev. A **90**, 023627 (2014).
[41] J.-S. Pan, X.-J. Liu, W. Zhang, W. Yi, and G.-C. Guo, Phys. Rev. Lett. **115**, 045303 (2015).
[42] L. Dong, C. Zhu, and H. Pu, Atoms **3**, 182 (2015).
[43] C. Kollath, A. Sheikhan, S. Wolff, and F. Brennecke, Phys. Rev. Lett. **116**, 060401 (2016).
[44] A. Sheikhan, F. Brennecke, and C. Kollath, Phys. Rev. A **93**, 043609 (2016).
[45] S. Gopalakrishnan, B. L. Lev, and P. M. Goldbart, Nat. Phys. **5**, 845 (2009).
[46] H. Talbot, Philos. Mag., Series 3 **9**, 401 (1836).
[47] T. Ackemann and W. Lange, Appl. Phys. B **72**, 21 (2001).
[48] G. Labeyrie, E. Tesio, P. M. Gomes, G.-L. Oppo, W. J. Firth, G. R. M. Robb, A. S. Arnold, R. Kaiser, and T. Ackemann, Nat. Photonics **8**, 321 (2014).
[49] M. Diver, G. R. M. Robb, and G.-L. Oppo, Phys. Rev. A **89**, 033602 (2014).
[50] G. R. M. Robb, E. Tesio, G.-L. Oppo, W. J. Firth, T. Ackemann, and R. Bonifacio, Phys. Rev. Lett. **114**, 173903 (2015).
[51] S. Gopalakrishnan, B. Lev, and P. Goldbart, Phys. Rev. A **82**, 043612 (2010).
[52] A. Wickenbrock, M. Hemmerling, G. R. M. Robb, C. Emary, and F. Renzoni, Phys. Rev. A **87**, 043817 (2013).
[53] A. J. Kollár, A. T. Papageorge, K. Baumann, M. A. Armen, and B. L. Lev, New J. Phys. **17**, 043012 (2015).
[54] A. J. Kollár, A. T. Papageorge, V. D. Vaidya, Y. Guo, J. Keeling, and B. L. Lev, arXiv:1606.04127 [Nat. Commun. (to be published)].
[55] S. Tewari, V. W. Scarola, T. Senthil, and S. Das Sarma, Phys. Rev. Lett. **97**, 200401 (2006).
[56] J. I. Cirac, P. Maraner, and J. K. Pachos, Phys. Rev. Lett. **105**, 190403 (2010).
[57] E. Zohar and B. Reznik, Phys. Rev. Lett. **107**, 275301 (2011).
[58] E. Zohar, J. I. Cirac, and B. Reznik, Phys. Rev. Lett. **109**, 125302 (2012).
[59] D. Banerjee, M. Dalmonte, M. Müller, E. Rico, P. Stebler, U.-J. Wiese, and P. Zoller, Phys. Rev. Lett. **109**, 175302 (2012).
[60] D. Banerjee, M. Bögli, M. Dalmonte, E. Rico, P. Stebler, U.-J. Wiese, and P. Zoller, Phys. Rev. Lett. **110**, 125303 (2013).
[61] M. J. Edmonds, M. Valiente, G. Juzeliūnas, L. Santos, and P. Öhberg, Phys. Rev. Lett. **110**, 085301 (2013).
[62] E. Zohar, J. I. Cirac, and B. Reznik, Phys. Rev. A **88**, 023617 (2013).
[63] E. Zohar, J. I. Cirac, and B. Reznik, Phys. Rev. Lett. **110**, 055302 (2013).

[64] K. Kasamatsu, I. Ichinose, and T. Matsui, Phys. Rev. Lett. **111**, 115303 (2013).
[65] E. Zohar, J. I. Cirac, and B. Reznik, Rep. Prog. Phys. **79**, 014401 (2016).
[66] P. Hauke, D. Marcos, M. Dalmonte, and P. Zoller, Phys. Rev. X **3**, 041018 (2013).
[67] L. Tagliacozzo, A. Celi, A. Zamora, and M. Lewenstein, Ann. Phys. (N.Y.) **330**, 160 (2013).
[68] D. Yang, G. Shankar Giri, M. Johanning, C. Wunderlich, P. Zoller, and P. Hauke, Phys. Rev. A **94**, 052321 (2016).
[69] E. A. Martinez, C. A. Muschik, P. Schindler, D. Nigg, A. Erhard, M. Heyl, P. Hauke, M. Dalmonte, T. Monz, P. Zoller, and R. Blatt, Nature (London) **534**, 516 (2016).
[70] D. Marcos, P. Rabl, E. Rico, and P. Zoller, Phys. Rev. Lett. **111**, 110504 (2013).
[71] D. Marcos, P. Widmer, E. Rico, M. Hafezi, P. Rabl, U.-J. Wiese, and P. Zoller, Ann. Phys. (N.Y.) **351**, 634 (2014).
[72] A. T. Papageorge, A. J. Kollár, and B. L. Lev, Opt. Express **24**, 11447 (2016).
[73] L. J. LeBlanc, M. C. Beeler, K. Jiménez-García, R. A. Williams, W. D. Phillips, and I. B. Spielman, New J. Phys. **17**, 065016 (2015).
[74] F. Schmidt, D. Mayer, M. Hohmann, T. Lausch, F. Kindermann, and A. Widera, Phys. Rev. A **93**, 022507 (2016).
[75] See Supplemental Material at http://link.aps.org/supplemental/10.1103/PhysRevLett.118.045302 for details of the reduction to effective 2D equations, details of the numerical simulation, a discussion of artificial magnetic field strength suppression in the geometry under consideration, and the evolution in real time.
[76] A. E. Siegman, *Lasers* (University Science Books, Sausolito, 1986).
[77] G. R. Dennis, J. J. Hope, and M. T. Johnsson, Comput. Phys. Commun. **184**, 201 (2013).